THE JOURNAL OF BIOLOGICAL CHEMISTRY VOL. 290, NO. 12, pp. 7634–7646, March 20, 2015
© 2015 by The American Society for Biochemistry and Molecular Biology, Inc. Published in the U.S.A.

Catecholamine Stress Hormones Regulate Cellular Iron Homeostasis by a Posttranscriptional Mechanism Mediated by Iron Regulatory Protein

*IMPLICATION IN ENERGY HOMEOSTASIS**

Received for publication, June 27, 2014, and in revised form, January 7, 2015 Published, JBC Papers in Press, January 8, 2015, DOI 10.1074/jbc.M114.592519

Nisha Tapryal[1], **Vishnu Vivek G, and Chinmay K. Mukhopadhyay**[2]

From the Special Centre for Molecular Medicine, Jawaharlal Nehru University, New Delhi-110 067, India

Background: The role of catecholamines in cellular iron homeostasis is not understood.
Results: Epinephrine and norepinephrine up-regulate transferrin receptor-1, inhibit ferritin expression, and increase mitochondrial iron content in hepatic and skeletal muscle cells.
Conclusion: Catecholamine stress hormones are novel regulators of cellular iron homeostasis.
Significance: Catecholamines may act to increase cellular iron content to meet an increased demand during stress.

Adequate availability of iron is important for cellular energy metabolism. Catecholamines such as epinephrine and norepinephrine promote energy expenditure to adapt to conditions that arose due to stress. To restore the energy balance, epinephrine/norepinephrine-exposed cells may face higher iron demand. So far, no direct role of epinephrine/norepinephrine in cellular iron homeostasis has been reported. Here we show that epinephrine/norepinephrine regulates iron homeostasis components such as transferrin receptor-1 and ferritin-H in hepatic and skeletal muscle cells by promoting the binding of iron regulatory proteins to iron-responsive elements present in the UTRs of transferrin receptor-1 and ferritin-H transcripts. Increased transferrin receptor-1, decreased ferritin-H, and increased iron-responsive element-iron regulatory protein interaction are also observed in liver and muscle tissues of epinephrine/norepinephrine-injected mice. We demonstrate the role of epinephrine/norepinephrine-induced generation of reactive oxygen species in converting cytosolic aconitase (ACO1) into iron regulatory protein-1 to bind iron-responsive elements present in UTRs of transferrin receptor-1 and ferritin-H. Our study further reveals that mitochondrial iron content and mitochondrial aconitase (ACO2) activity are elevated by epinephrine/norepinephrine that are blocked by the antioxidant *N*-acetyl cysteine and iron regulatory protein-1 siRNA, suggesting involvement of reactive oxygen species and iron regulatory protein-1 in this mechanism. This study reveals epinephrine and norepinephrine as novel regulators of cellular iron homeostasis.

Iron is one of the most essential micronutrients required for the body to maintain energy homeostasis (1). It participates in many enzymic electron transfer reactions due to its redox nature; however, it may generate the potentially dangerous hydroxyl radical in the presence of reactive oxygen species (ROS)[3] (2). Thus, iron homeostasis genes are tightly regulated mostly at the posttranscriptional level in mammalian cells (3). During cellular iron demand, transferrin receptor 1 (TfR1) expression is increased by an mRNA stability mechanism due to binding of iron regulatory proteins (IRPs) to multiple iron regulatory elements (IRE) present in its 3′-UTR. Simultaneously, expression of the iron storage protein ferritin (Ft) is inhibited by a translational mechanism due to binding of IRPs to a single IRE present in 5′-UTR of ferritin to satisfy the other cellular iron demand essential for maintaining homeostasis. Among two cytosolic IRPs, IRP1 is an Fe-S cluster containing bifunctional protein. It binds IRE-containing mRNAs in iron-depleted cells or acts as a cytosolic aconitase (ACO1) in iron-repleted cells (4). Other than iron depletion, ROS and NO also convert ACO1 into IRP1 (5–7). Unlike IRP1, IRP2 is devoid of Fe-S cluster or aconitase activity and mainly regulated due to the alteration of cellular iron pool by a posttranslational protein stability mechanism (8). A recent finding suggests that IRPs also influence mitochondrial iron homeostasis and function in hepatocytes (9).

In mammals, various psychosocial and physical stresses activate the peripheral sympatho-adrenomedullary and central catecholaminergic systems to elevate secretion of epinephrine (EPI) and norepinephrine (NE) in the circulation. These stress hormones, more commonly known as catecholamines, trigger a series of biological reactions, including increased rate of energy metabolism (10, 11), to prepare the organism to overcome or to adapt to the stressful events. During chronic or acute stress, EPI/NE concentration could be elevated up to 80–100 times in plasma as compared with 3–5 nM EPI/NE in normal condition (12–14). Skeletal muscle cells may be exposed to a far higher concentration of catecholamines as they are present abun-

* This work was supported by the Council of Scientific and Industrial Research (CSIR) of India.
[1] Recipient of a fellowship from the CSIR.
[2] To whom correspondence should be addressed: Special Centre for Molecular Medicine, Jawaharlal Nehru University, New Delhi-110 067, India. Tel.: 91-11-2673-8738; Fax: 91-11-2674-7511; E-mail: ckm2300@mail.jnu.ac.in.

[3] The abbreviations used are: ROS, reactive oxygen species; TfR1, transferrin receptor 1; IRP, iron regulatory protein; IRE, iron regulatory element(s); Ft, ferritin; EPI, epinephrine; NE, norepinephrine; ACO1, cytosolic aconitase; ACO2, mitochondrial aconitase; Fpn, ferroportin; DCFH-DA, ′,7′-dichlorofluorescein diacetate; qRT-PCR, quantitative RT-PCR; DFO, desferrioxamine; NAC, *N*-acetyl cysteine; Mit-Fe, mitochondrial iron; mut, mutant; TCA, tricarboxylic acid.

dantly in neuromuscular junctions that connect the nervous system to the muscular system. It is estimated that perisynaptic catecholamine concentrations are in the range of 30–400 μM (15, 16), whereas within the synaptic cleft, they may reach up to mM concentrations (16). Catecholamines enhance glycogenolysis in the liver to increase glucose release in the bloodstream to compensate the extra glucose consumption by various organs, including brain, heart, and muscles, for enhanced ATP production. During stress response, a 40% increase in energy expenditure was reported in skeletal muscles alone (17). Because rate-limiting enzymes of energy-generating pathways such as the TCA cycle and mitochondrial electron transport chain are dependent on iron (18), during stress conditions leading to higher catecholamine release, there should be an alteration in cellular iron requirement in targeted cells. However, so far, not much has been explored to understand cellular iron homeostasis during catecholamine exposure.

Here we show that EPI and NE promote IRE-IRP interaction in ROS-sensitive mechanism to regulate TfR1 mRNA stability and ferritin translation in the liver and muscle cells to increase mitochondrial iron content. This study establishes EPI and NE as novel regulators of iron homeostasis in hepatic and muscle cells.

EXPERIMENTAL PROCEDURES

Cell Culture—The human hepatoma HepG2 cell and mouse skeletal muscle C2C12 cell were grown at 37 °C in 5% CO_2 atmosphere in Dulbecco's modified Eagle's medium supplemented with 10% heat-inactivated fetal bovine serum, 100 units/ml penicillin, 100 μg/ml streptomycin, and 2 mM L-glutamine. Cells (50–60% confluence) were treated with either (−)-epinephrine bitartrate salt (Sigma) or (−)-norepinephrine bitartrate salt (Sigma) in serum-free conditions.

Animals—BALB/C mice (22–25 g) were housed three per group, in a room (22 ± 5 °C) with an alternating 12-h light-dark cycle. Food and water were available *ad libitum*. Catecholamines were dissolved in ice-cold vehicle (0.9% NaCl containing 18 mg liter^{-1} ascorbic acid) immediately before administration and protected from light to minimize oxidation. The mice were injected intraperitoneally with vehicle only, 0.05 mg kg^{-1} of epinephrine or norepinephrine. Mice were sacrificed (6 h); livers and skeletal muscles were collected for further processing. Animals were treated according to guidelines of the Institutional Animal Ethics Committee.

Isolation of Mitochondrial and Cytosolic Extracts for Aconitase Assays—Cytoplasmic and mitochondrial fractions were isolated as described previously (19, 20). Briefly, cells and tissues were kept in ice-cold buffer containing 250 mM sucrose, 10 mM KCl, 1.5 mM $MgCl_2$, 1 mM DTT, 20 mM HEPES (pH 7.4), and 1× protease inhibitor cocktail (Roche Diagnostics). Tissues were homogenized with a Potter-Elvehjem system. Cell suspension and tissue homogenates were passed through a 30-gauge needle 10–12 times and subjected to centrifugation at 2,000 × *g* for 5 min at 4 °C to separate the nuclear fraction. Supernatants were again centrifuged at 10,000 × *g* for 15 min, and then the cytoplasmic fraction was collected, leaving the mitochondrial pellet intact. The pellet was suspended in buffer containing 0.2% Triton X-100, 100 mM NaCl, and 100 mM Tris-HCl (pH 7.5) for 20 min on ice and centrifuged at 10,000 × *g* for 15 min. The purity of the mitochondrial fraction was determined by immunoblotting with GAPDH antibody (Santa Cruz Biotechnology), and the presence of mitochondrial fraction was confirmed by using a porin antibody (Santa Cruz Biotechnology). Protein concentration was estimated by protein assay reagent (Bio-Rad). The aconitase activity was determined in respective cellular fractions by monitoring the disappearance of *cis*-aconitate at 240 nM at 25 °C for 20 min as described previously (19, 20).

Estimation of Mitochondrial Iron—Mitochondrial suspension (10 μl) was mixed with 90 μl of 10% HCl + 10% TCA and incubated overnight at 45 °C as described earlier (9). The samples were centrifuged for 10 min at 10,000 × *g*, and the supernatant was incubated for 10 min with 5 volumes of 3 M sodium acetate, 0.01% bathophenanthroline-disulfonic acid, and 0.1% thioglycolic acid. The optical density was measured at 535 nm after 15 min. For each sample, the blank absorbance was determined by omitting the bathophenanthroline chromogen. The amount of iron was inferred from the serial dilution of a standard iron solution (iron atomic spectroscopy standard, Fluka).

Western Blot Analysis—Cell lysates were prepared from untreated and treated cells as described elsewhere (19). Tissue lysates were prepared by homogenization with a Potter-Elvehjem system in a lysis buffer containing 50 mM Hepes (pH 7.5), 150 mM NaCl, 1 mM EDTA, 2 mM sodium vanadate, 1 mM phenylmethylsulfonyl fluoride, 0.5% Nonidet P-40, and 1× protease inhibitor cocktail and subsequent centrifugation at 10,000 × *g* for 15 min. To determine the IRP1 and IRP2 expressions, cell lysates/cytosolic extracts were prepared in buffer containing 0.5 mM DTT. Immunoblot analysis was performed using supernatants (40 μg). Antigens were detected using mouse monoclonal anti-TfR1 (Invitrogen), anti-ferritin-H, and anti-aconitase 2 (both from Cell Signaling), and anti IRP1/2, anti-GAPDH, anti-porin, anti-ferroportin, and anti-actin antibodies (all from Santa Cruz Biotechnology). Immunoreactive bands were detected with HRP-conjugated secondary antibodies using ECL (Amersham Biosciences).

RNA Isolation and Real-time Quantitative PCR Analysis—Cells or tissues, washed with ice-cold phosphate-buffered saline, were lysed in TriPure (Roche Applied Science), and total RNA was isolated according to the manufacturer's specifications. Total RNA (2 μg) was reverse-transcribed at a final volume of 20 μl by using the High-Capacity cDNA reverse transcription kit (Applied Biosystems). Two μl of the RT products were amplified and quantified in the Applied Biosystems 7500 fast real-time PCR system by using SYBR Green real time PCR master mix (Applied Biosystems) and gene-specific primers (TfR1: 5′-GCT TGA AGA TCG TTA G-3′ and 5′-CTA ACA CAG TAA AGG TC-3′; Ft-H, 5′-CGT TCT CGC CCA GAG TCG CC-3′ and 5′-ACC GTG TCC CAG GGT GTG CT-3′; and actin, 5′-GAC ATG GAG AAG ATC-3′ and 5′-GAA TGT AGT TTC ATG-3′. Actin levels were used as the endogenous controls. To examine the identity of the PCR, the product melting curve was analyzed regularly. PCR products were also verified on agarose gel to examine the correct size of the PCR products. Relative gene expression was calculated using the comparative CT method formula: relative quantification = $2^{-\Delta\Delta CT}$.

Reporter Construct Preparation and Reporter Assay—A 536-bp-long 5′-flanking region of TfR1 (−491 to + 45 of transcription start site) was cloned upstream of the luciferase gene in the

reporter vector pGL3-basic. Similarly, 5′-UTR of the Ft-H chain containing the single IRE sequence was PCR-amplified and cloned upstream of the luciferase gene in the pGL3-control vector. All constructs were verified by sequencing. TfR1 promoter or Ft-H-IRE construct (1 μg) was transfected into HepG2 cells using FuGENE 6 (Roche Applied Science). To monitor transfection efficiency, a reporter gene construct (0.25 μg) containing β-galactosidase downstream of a CMV promoter was also co-transfected simultaneously. After recovery, cells were incubated with catecholamines in serum-free medium. Luciferase activity was examined in cell extracts using the luciferase assay kit (Promega) and normalized to β-galactosidase activity (Invitrogen).

Preparations of Cytosolic Extracts and RNA Gel-shift Analysis—RNA gel-shift analysis for TfR1-IRE was performed using cytosolic extracts as described earlier (19, 21, 22). RNA-protein complexes were analyzed in a 5% non-denaturing PAGE, and gels were dried followed by autoradiography.

Ferritin IRE containing 28 nucleotides with a hairpin loop with an internal loop or bulge plays a crucial role in the binding of IRP1 and IRP2. It is well established that G18A point mutation of IRE abolishes the interaction with IRPs (23, 24). For RNA-EMSA with ferritin IRE (Ft-IRE), double-stranded DNA template harboring a recognition sequence for T7 RNA polymerase followed by a ferritin IRE coding region was prepared by annealing the synthetic sense and antisense oligonucleotides using a strategy described earlier (25). For that procedure, the following oligonucleotides were used. 1) To prepare wild type IRE coding DNA template, we used: sense WT, 5′-ATGTAATACGACTCACTATAGGGCGATTTCCTGCTTCAACAGTGCTTGGACGGAAC-3′; and antisense WT, 5′-GTTCCGTCCAAG**C**ACTGTTGAAGCAGGAAA*TCGCCCTATAGTGAGTCGTATTA*CAT-3′; 2) To prepare G18A mutant IRE coding DNA template, we used: sense mut, 5′-ATGTAATACGACTCACTATAGGGCGATTTCCTGCTTCAACAGTACTTGGACGGAAC-3′, and antisense mut, 5′-GTTCCGTCCAAG**T**ACTGTTGAAGCAGGAAA*TCGCCCTATAGTGAGTCGTATTA*CAT-3′. The underlined sequences represent Ft-IRE sequence. The nucleotide sequences in italics represent T7 RNA polymerase binding sequence. In wild type Ft-IRE, the nucleotide G was shown as C in the antisense sequence in bold. The nucleotide G was replaced with A (shown as bold T in antisense sequence) for preparing mutated probe (Ft-IRE-mut).

These probes for RNA EMSA were prepared by *in vitro* transcription of the respective double-stranded templates in the presence of [α-^{32}P]UTP (Board of Radiation and Isotope Technology (BRIT), Mumbai, India) by T7 RNA polymerase using an *in vitro* transcription kit (Roche Applied Science). Purified ^{32}P-labeled ferritin IREs were incubated with 10 μg of cytosolic extracts in a binding buffer containing 10 mM Tris-Cl buffer (pH 7.6), 15 mM KCl, 5 mM $MgCl_2$, 0.1 mM dithiothreitol, 10 units of RNase inhibitor, and 0.2 mg/ml yeast tRNA in a 30-μl reaction volume. After a 15-min incubation in ice, 1 unit of RNase T1 was added for 10 min followed by 100 mg of heparin/ml of treatment for another 10 min. RNA-protein complexes were resolved on a 5% non-denaturing polyacrylamide gel at 120 V using 0.5× Tris-borate-EDTA as the running buffer at 4 °C. The gels were dried, and radiolabeled bands were detected by autoradiography.

To perform an RNA gel-shift assay with ferroportin (Fpn)-IRE, a pcDNA3 plasmid construct with a 267-nucleotide Fpn 5′-UTR containing an IRE was linearized and transcribed using an *in vitro* transcription kit (Roche Applied Science). Using ^{32}P-labeled Fpn-5′-UTR, an RNA gel-shift assay was performed. For that, 10 μg of cytoplasmic extracts isolated from untreated and EPI/NE (30 μM)-treated cells were incubated with radiolabeled Fpn-5′-UTR probe. RNA-protein complexes were resolved by 5% non-denaturing polyacrylamide gels, dried, and subjected to autoradiography.

Detection of Intracellular ROS Generation—Subconfluent HepG2 cells were treated with EPI/NE (30 μM). The fluorescent probe, 2′,7′-dichlorofluorescein diacetate (DCFH-DA, 5 μM), was used to monitor the intracellular generation of ROS as described earlier (21). Briefly, cells were incubated with medium alone and EPI/NE for 10 min followed by the addition of DCFH-DA. After 20 min, cells were washed with 1× PBS. The fluorescence intensities of cells were captured by Nikon upright fluorescence microscope model 80i and analyzed with the ImageJ software (National Institutes of Health).

Knocking Down of IRP1 by siRNA—HepG2 cells were transfected with the IRP1 siRNAs (IRP1 siRNA-1: SASI_Hs01_00138944 and IRP1 siRNA-2: SASI_Hs01_00138945) and transfected with control siRNA (SIC001) (10 nM) in 6/12-well plates using the N-TER^{TM} nanoparticle siRNA transfection system as per the manufacturer's protocol (Sigma). After transfection, Western blot analyses were performed for IRP1 and actin as described before.

Statistical Analysis—All experiments were performed at least three times with similar results, and representative experiments are shown. Densitometric results are normalized with respect to internal controls and expressed relative to the results in untreated controls. Results are expressed as means ± S.D.

RESULTS

EPI and NE Regulate TfR1 and Ft-H in Hepatic and Muscle Cells—To determine the influence of EPI and NE on iron homeostasis, we examined the expressions of TfR1 and Ft-H in human hepatic HepG2 and mouse skeletal muscle C2C12 cells by Western blot analysis. In both cell types, TfR1 expression was increased with increasing concentrations (0–30 μM) of EPI or NE (Fig. 1, *A–D*). We limited our study up to 30 μM catecholamine treatment due to earlier reports of norepinephrine receptor-mediated NE transport in mammalian peripheral cells in this concentration (26, 27). TfR1 expression was increased in HepG2 cells at a maximum of ~3.6-fold (Fig. 1, *A* and *B*) and increased at a maximum of ~2.5-fold in C2C12 cells (Fig. 1, *C* and *D*) by EPI or NE treatment. Similar EPI/NE treatment decreased Ft-H protein expression more than 70% as compared with untreated HepG2 and C2C12 cells (Fig. 1, *A–D*). We also determined the effect of catecholamines on expression of cellular iron exporter Fpn. We did not observe any alteration of ferroportin expression in response to EPI (0–30 μM) (Fig. 1*E*) or NE (data not shown). When BALB/C mice were injected with a single intraperitoneal dose of either EPI or NE, up to a 70% increase of TfR1 and an ~60% decrease in Ft-H expressions were detected in the liver as compared with placebo-injected mice (Fig. 1*F*).

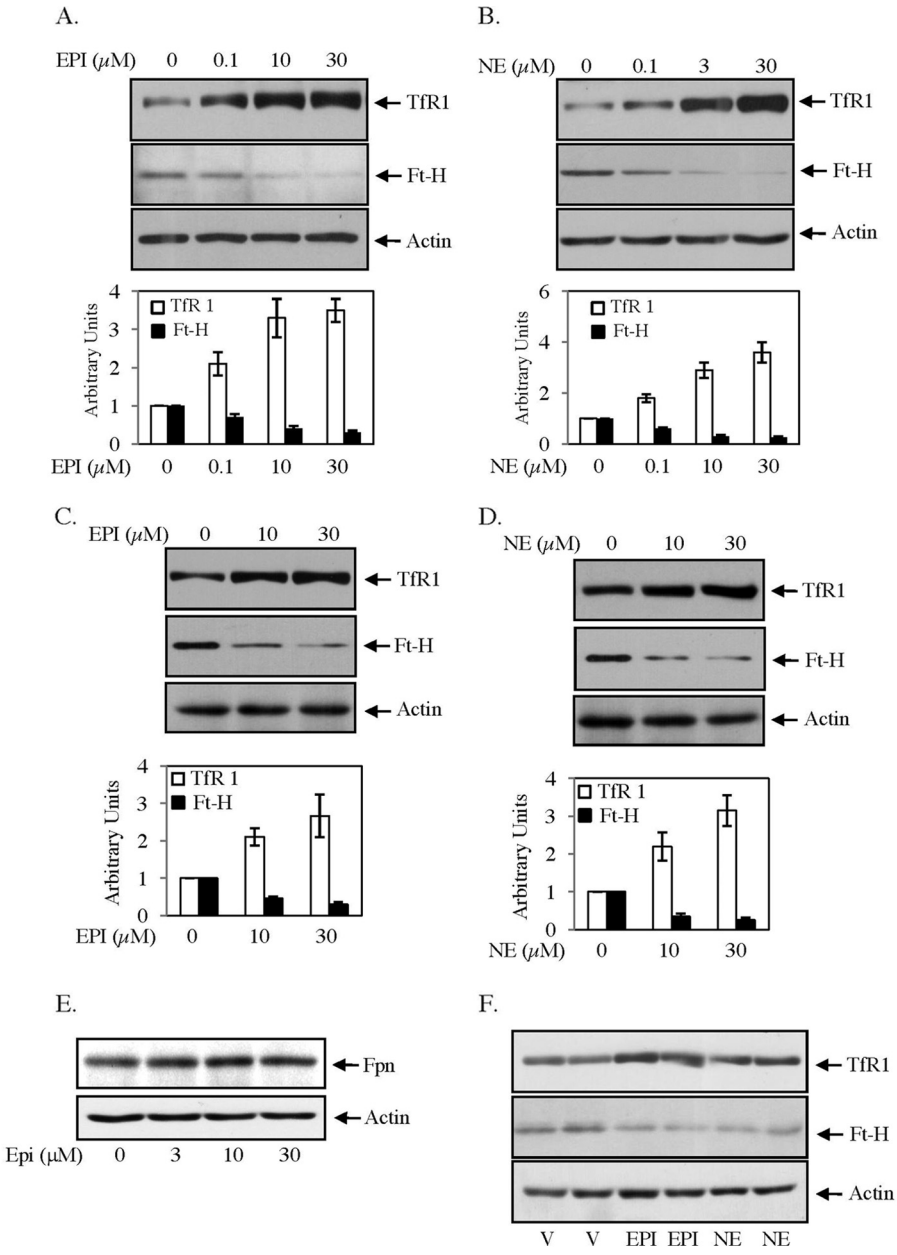

FIGURE 1. **EPI/NE regulates TfR1 and Ft-H expressions in liver and muscle cells.** *A* and *B*, expressions of TfR1 (*upper panel*), Ft-H (*middle panel*), and actin (*lower panel*) were detected by Western blot analyses in EPI-treated (*A*) (0–30 μM, 16 h) and NE-treated (*B*) (0–30 μM, 16 h) HepG2 cell lysates. *Bottom panels* are quantifications of the Western blot analyses of three independent experiments. *Error bars* indicate S.D. *C* and *D*, similarly, TfR1 (*upper panel*), Ft-H (*middle panel*), and actin (*lower panel*) expressions were analyzed by Western blotting in C2C12 cells stimulated for 16 h with EPI (0–30 μM) (*C*) and NE (0–30 μM) (*D*). *Bottom panels* are quantifications of Western blot analyses of three independent experiments, and *error bars* indicate S.D. *E*, HepG2 cells were treated with EPI (0–30 μM) for 16 h, and Western blot analysis was performed using Fpn (*upper panel*) and actin (*lower panel*) antibody. The result represents one of the three independent experiments. *F*, TfR1 (*upper panel*), Ft-H (*middle panel*), and actin (*lower panel*) expressions were detected by Western blot analyses in liver homogenate isolated from vehicle (*V*)-, EPI-, and NE-injected mice (6 h). Each lane represents homogeneous mixtures isolated from three animals. At least three independent experiments were performed for each group.

To understand the mechanism further, expressions of TfR1 and Ft-H transcripts were examined by qRT-PCR. EPI or NE treatment increased TfR1 mRNA in a concentration-dependent manner in both HepG2 and C2C12 cell types, whereas no significant change was detected for Ft-H mRNA (Fig. 2, *A–D*). A comparable increase in TfR1 mRNA level with the increased protein level was detected in all conditions mentioned above. We observed a maximum increase in TfR1 mRNA level in NE-treated HepG2 cells between 8 and 16 h (data not shown). An ~1.9-fold increase in TfR1 mRNA level was detected in the liver and muscle of EPI-injected mice, whereas Ft-H transcript remained unaltered (Fig. 2, *E* and *F*).

EPI and NE Regulate TfR1 and Ft-H at Posttranscriptional Level—To determine the mechanism of increase in TfR1 mRNA, we first examined its promoter activity in a reporter gene assay. TfR1 promoter region cloned in to pGL3 vector upstream of luciferase gene was transfected into HepG2 cells. Then transfected cells were treated with EPI/NE or hypoxia mimetic $CoCl_2$, and a luciferase assay was performed in cell lysates after 16 h of treatment. No significant change in pro-

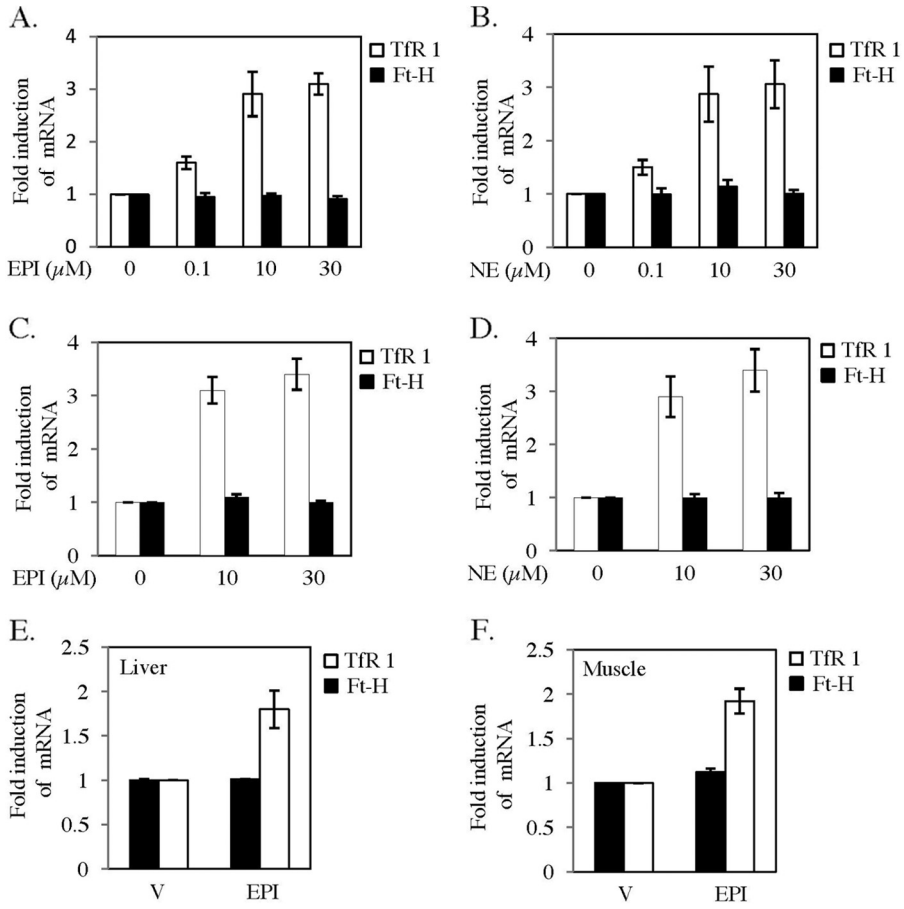

FIGURE 2. **EPI and NE regulate TfR1 but not Ft-H transcripts.** *A* and *B*, HepG2 cells were treated with EPI (0–30 μM) (*A*) and NE (0–30 μM) (*B*) for 12 h. Quantitative RT-PCR was performed for TfR1, Ft-H, and actin. *C* and *D*, similarly, C2C12 cells were treated for 12 h with EPI (0–30 μM) (*C*) and NE (0–30 μM) (*D*), and qRT-PCR was performed for TfR1, Ft-H, and actin. *E* and *F*, qRT-PCR was performed with the RNA isolated from liver (*E*) and muscle (*F*) of vehicle (*V*)- or EPI-injected mice using TfR1-, Ft-H-, and actin-specific primers. Each data point represents the mean ± S.D. from three independent experiments.

moter activity was detected after EPI or NE treatment, but cobalt chloride increased promoter activity by more than 2.5-fold in HepG2 cells (Fig. 3*A*) as reported earlier (28). To verify the effect of EPI/NE on TfR1 mRNA stability, we measured its half-life in EPI- or NE-treated HepG2 cells. Initially, cells were either kept untreated or treated with EPI/NE (30 μM), and after 6 h, all cells were treated with transcription blocker actinomycin D. RNA was isolated after 0, 1, 2, and 3 h of actinomycin D addition, and TfR1 mRNA expression was detected by qRT-PCR. Half-life of TfR1 mRNA in untreated cells was detected at about 2 h as reported earlier (19, 22, 29), and was increased significantly in EPI- or NE-treated cells (Fig. 3*B*). These data confirmed that both EPI and NE regulate TfR1 expression by promoting mRNA stability. TfR1 mRNA stability is usually regulated by binding of IRPs to IREs present in its 3′-UTR. Similarly, ferritin translation is also regulated by the single IRE present in its 5′-UTR. Decreased Ft-H protein levels, but unaltered levels of Ft-H mRNA in response to EPI/NE, suggest translational blocking mediated by its 5′-UTR. To examine that, we transfected C2C12 cells with pGL3-control vector or pGL3-control vector in which 5′-UTR of ferritin was cloned upstream of the luciferase gene (Fig. 3*C*, *upper panel*). Transfected cells were then treated with EPI/NE or kept untreated. Result showed significant inhibition (up to 85%) of luciferase activity with increasing concentration of EPI or NE treatment for ferritin-5′-UTR containing vector, but no effect was detected with only pGL3-control-transfected cells (Fig. 3*C*, *lower panels*).

Catecholamines Increase IRE-IRP Interaction—Our earlier results suggest that EPI/NE may regulate TfR1 and Ft-H by modulating IRE-IRP interaction. To verify that, we examined IRE-IRP interaction in NE-treated HepG2 cells. When ^{32}P-labeled TfR1-IRE probe was incubated with cytosolic extracts isolated from untreated or NE-treated cells (19, 21, 22), an increased IRE binding activity was detected with increasing concentrations of NE (0–30 μM) (Fig. 4*A*). The iron chelator desferrioxamine (DFO) was used as a positive control (Fig. 4*A*). To examine whether the increased binding of IRE was due to IRPs, an equal amount of cytosolic extracts from control-, EPI-, or DFO-treated HepG2 cells was incubated with ^{32}P-labeled TfR1-IRE in the presence of IRP1 or/and IRP2 antibody. EPI-induced IRE binding complex was reduced/disappeared in the presence of both IRP1 and IRP2 antibodies when used individually or together, whereas nonspecific Fpn antibody did not show any effect on increased IRE complex formation (Fig. 4*B*). A similar result of reducing/disappearing of the IRE binding complex induced by the iron chelator DFO was also detected with IRP1 or IRP2 antibody (Fig. 4*B*), suggesting that the induced complex might be due to IRPs.

To further verify that EPI/NE blocked Ft-H translation due to increased IRP binding to its 5′-UTR-IRE, cytosolic extracts

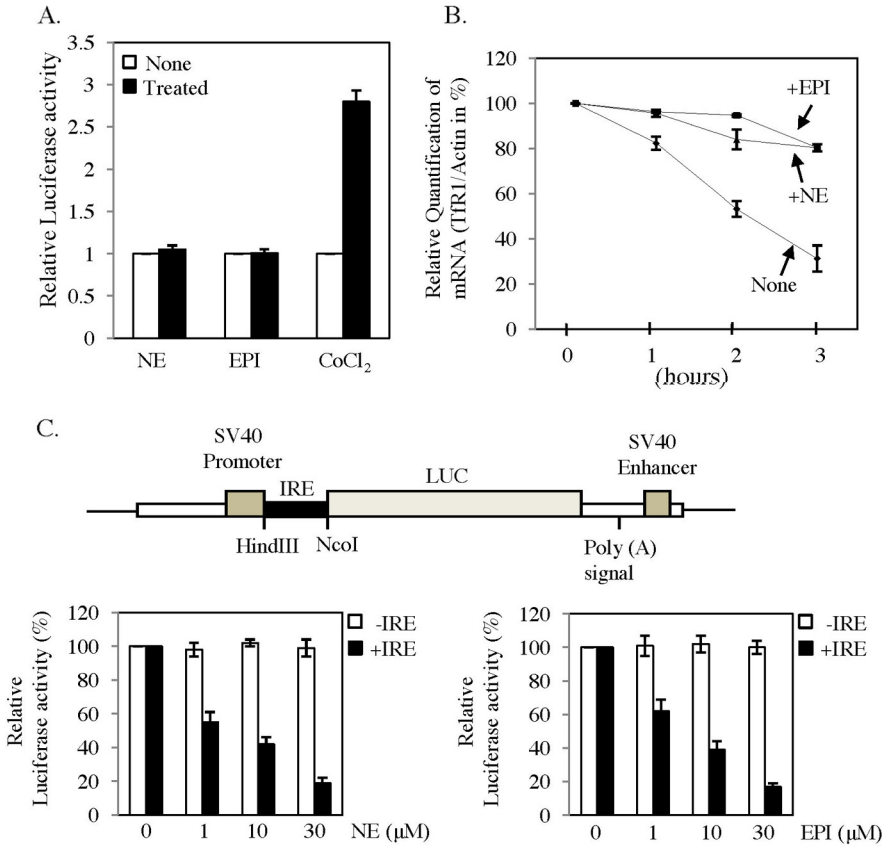

FIGURE 3. **Catecholamines increase TfR1 mRNA stability and block Ft-H translation.** *A*, effect of EPI and NE on TfR1 promoter activity. The mouse TfR1 promoter containing luciferase construct was transiently transfected to HepG2 cells along with CMV promoter containing β-galactosidase. After recovery, cells were kept untreated or treated with 30 μM EPI/NE. After 16 h, luciferase activity was measured in cell lysates and normalized with β-galactosidase activity. Cobalt chloride (100 μM) was used as a positive control. Results represent ± S.D. of three independent experiments performed in triplicates. *B*, effect of EPI/NE on TfR1 mRNA stability. HepG2 cells were treated with medium alone or EPI/NE (30 μM) for 6 h followed by 7.5 μg/ml actinomycin D treatment. Subsequently, total RNA was isolated after 0, 1, 2, and 3 h of actinomycin D treatment, and qRT-PCR was performed for TfR1 and actin. The figure represents data from three independent experiments. *C*, the *upper panel* shows the schematic diagram of the construct made in the pGL3-Control vector in which the 5′-UTR of Ft-H containing IRE was cloned upstream of luciferase gene. C2C12 cells were transfected with the same plasmid or only with pGL3-control vector along with β-galactosidase containing plasmid and then treated with EPI/NE (0–30 μM) for 16 h. Luciferase and β-galactosidase activities were measured in cell lysates and normalized (*lower panels*). *Error bars* represent ±S.D. from three independent experiments performed in triplicates.

from untreated and EPI-, NE-, or DFO-treated HepG2 cells were incubated with ^{32}P-labeled Ft-IRE, and an RNA gel-shift assay was performed. A strong increase in IRE binding activity was detected with EPI, NE, or positive control DFO (Fig. 4*C*). Ferritin-IRE is a conserved sequence of a 28-nucleotide-containing hairpin loop in which binding of IRPs is dependent on the presence of G at position 18 (23, 24). Mutation of this G to A is known to abolish the IRP binding completely (24). Because the RNA gel-shift assay with TfR1-IRE using IRP1 and/or IRP2 antibody (Fig. 4*B*) was suggestive but not confirmatory of IRPs binding to IRE, we used G to A mutation of the Ft-IRE probe to examine the specificity of the IRP binding. Thus, when ^{32}P-labeled Ft-IRE-mut probe was incubated with cytosolic extracts from untreated or EPI-, NE-, or DFO-treated HepG2 cells, no IRE binding was detected (Fig. 4*C*). A similar increase in IRP binding to the Ft-IRE was also obtained with cytosolic extract of EPI/NE/DFO-treated C2C12 cells, but not with the Ft-IRE-mut probe (Fig. 4*D*). These results confirmed that EPI/NE could induce IRE-IRP complex formation. Interestingly, ferroportin-IRE did not show any increased binding with cytosolic extract isolated from EPI/NE-treated HepG2 cells (Fig. 4*E*). Increased Ft-IRE complex formations were detected with cytosolic extracts isolated from the liver of EPI/NE-injected mice, but the complex formation was completely lost when Ft-IRE-mut probe was used (Fig. 4*F*). Similarly, cytosolic extracts isolated from skeletal muscle of EPI/NE-injected mice showed increased IRE-IRP interaction (Fig. 4*G*). All these results strongly suggest that EPI/NE modulate IRPs binding to IREs both *in vitro* and *in vivo*.

Catecholamines Induce IRE-IRP Interaction Mediated by ROS—To determine the mechanism of EPI/NE-induced activation of IRPs, we initially verified expressions of IRPs by immunoblot analysis. EPI/NE treatment did not show any significant change in IRP1 or IRP2 expression (Fig. 5, *A* and *B*), suggesting the conversion of ACO1 to the high affinity RNA binding IRP1 form. Therefore, we determined cytosolic aconitase activity in EPI/NE-treated HepG2 cells. We detected a dose-dependent decrease in aconitase activity with increasing concentrations of EPI or NE treatment (Fig. 5*C*). We also determined IRP1 and IRP2 expressions in cytosolic extracts of liver and muscle tissues of EPI/NE-injected mice and found no detectable change by immunoblot analysis as compared with vehicle-injected mice (Fig. 5, *D* and *E*). However, cytosolic aconitase activity was decreased about 50–55% in the liver and about 55–60% in muscle of EPI/NE-injected mice (Fig. 5*F*).

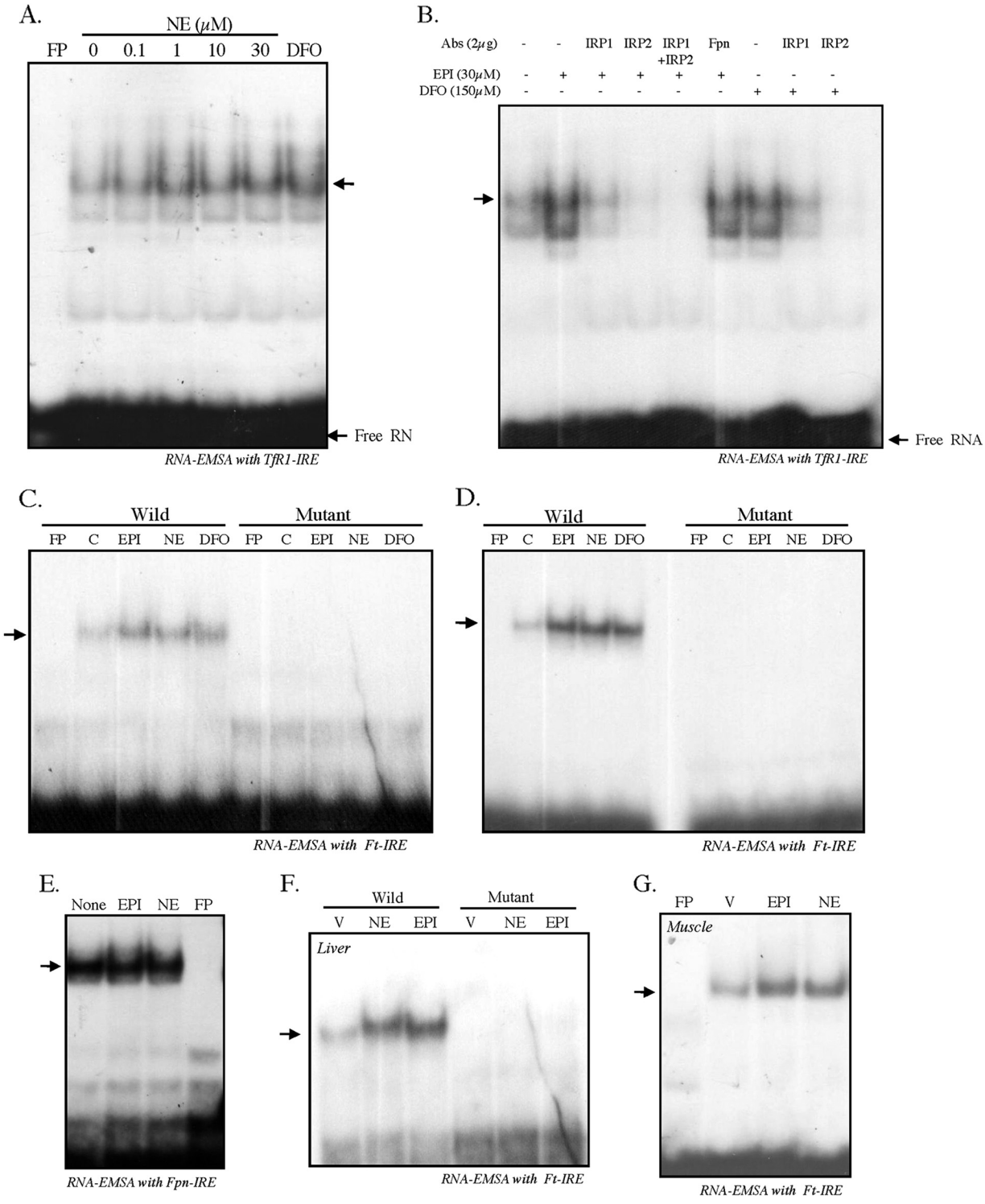

FIGURE 4. **Catecholamines promote IRE-IRP interaction.** *A*, RNA-EMSA was performed to assess IRE-IRP interaction in NE-treated (0–30 μM, 8 h) HepG2 cells. Cytosolic extracts (10 μg) were incubated with ^{32}P-labeled TfR1-IRE probe, and the RNA-protein complexes were separated on non-denaturing polyacrylamide gels. Cytosolic extract from DFO (150 μM)-treated cells was used as positive control. *B*, 2 μg of IRP1 or IRP2 antibody (*Abs*) alone or together were added along with the cytosolic extracts isolated from EPI-treated HepG2 cells just prior to the addition of radiolabeled IRE probe. Similarly, IRP1 or IRP2 antibody was added in DFO-treated cytosolic extract, and gel-shift analysis was performed. Fpn antibody was added to EPI-treated cytosolic extract as nonspecific control antibody. *C*, RNA-EMSA was performed with cytosolic extracts from untreated, EPI/NE (0.1 μM)-, or DFO (75 μM)-treated HepG2 cells incubated with ^{32}P-labeled Ft-IRE probe (*Wild*) or ^{32}P-labeled Ft-IRE-mut probe (*Mutant*). *D*, similarly, RNA-EMSA was performed with cytosolic extracts from untreated, EPI/NE (1 μM)- or DFO (100 μM)-treated C2C12 cells incubated with ^{32}P-labeled Ft-IRE probe or ^{32}P-labeled Ft-IRE-mut probe. *E*, RNA-EMSA was performed using radiolabeled RNA probe corresponding to the 267-nucleotide Fpn 5′-UTR after incubating with cytoplasmic extracts isolated from untreated and EPI/NE (30 μM)-treated HepG2 cells. RNA-protein complexes were resolved by 5% non-denaturing polyacrylamide gels, and gels were dried and subjected to autoradiography. *C*, control. *F*, RNA-EMSA was performed using ^{32}P-labeled Ft-IRE or ^{32}P-labeled Ft-IRE-mut probe with cytosolic extracts isolated from livers of vehicle (*V*)-, EPI-, or NE-injected mice. *G*, similarly, RNA-EMSA was performed using ^{32}P-labeled Ft-IRE probe with cytosolic extracts isolated from skeletal muscle of vehicle-, EPI-, or NE-injected mice. In all cases, *FP* denotes radiolabeled Ft-IRE probe without incubation of any cytosolic extract. Each experiment was performed at least three times independently with similar results.

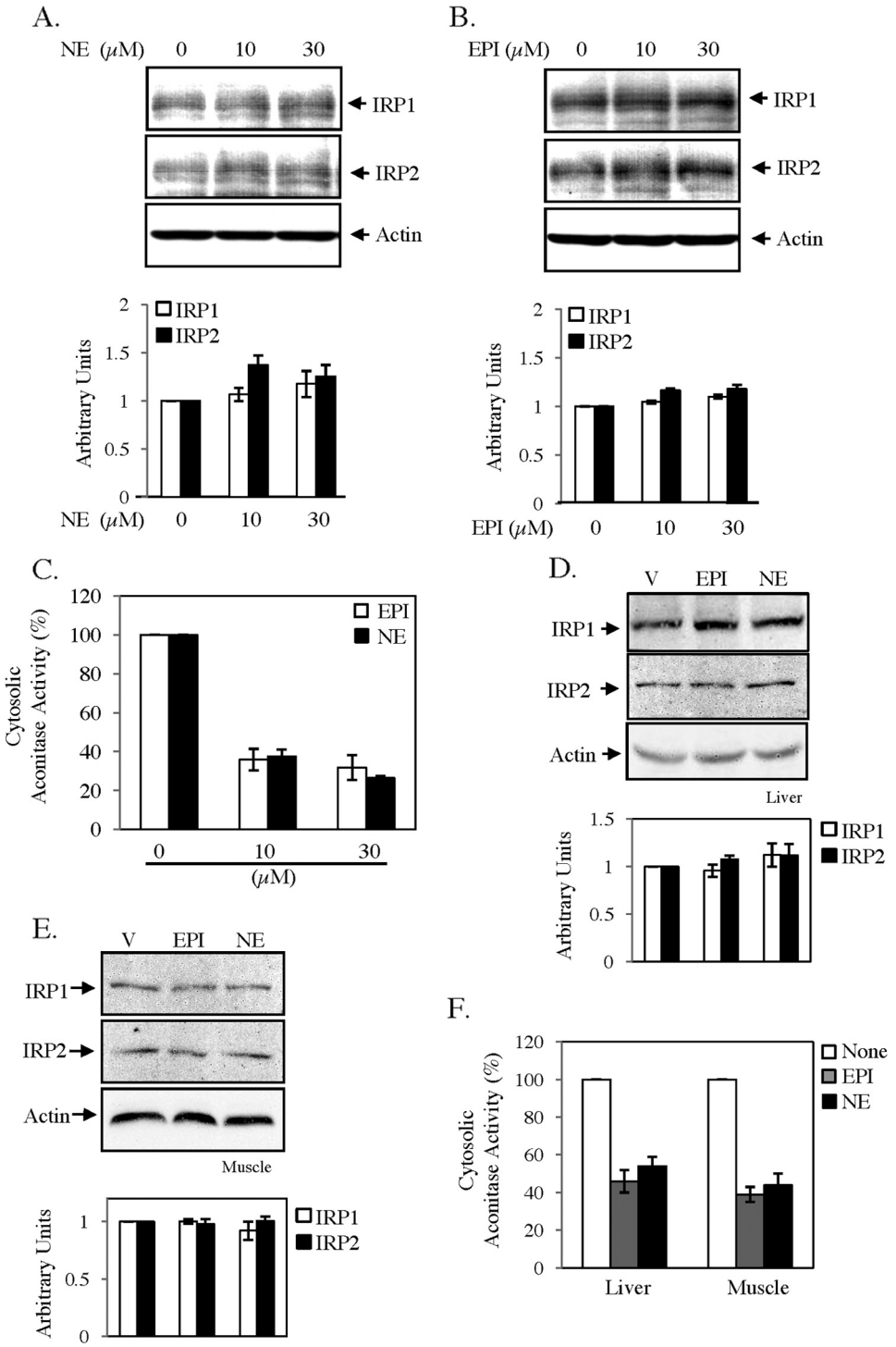

FIGURE 5. **Catecholamines regulate cytosolic aconitase activity.** *A* and *B*, HepG2 cells were treated with the indicated concentrations of NE (*A*) and EPI (*B*) for 10 h. Subsequently, cytosolic extracts were subjected to Western blot analysis using IRP1, IRP2, or actin antibodies. Specific bands were quantified, and results after normalization with actin are presented (*bottom panels*). *C*, aconitase assay was performed with cytosolic extracts of EPI/NE (0–30 μM)-treated HepG2 cells. *Error bars* indicate S.D. from three independent experiments. *D* and *E*, cytosolic extracts isolated from liver (*D*) and skeletal muscle tissue (*E*) of vehicle (*V*)-, EPI-, and NE-injected mice were subjected to Western blot analysis using IRP1, IRP2, or actin antibodies. Specific bands were quantified, and results after normalization with actin are presented (*bottom panels*). *F*, similarly, aconitase activity was determined in cytosolic extracts isolated from liver and skeletal muscle of vehicle- and EPI/NE-injected animals. *Error bars* indicate S.D. from three independent experiments.

Conversion of cytosolic aconitase to IRE binding IRP1 is usually promoted by depletion of cellular labile iron pool or increased ROS or NO generation (30, 31). We did not detect any change in calcein-sensitive labile iron pool in either HepG2 or C2C12 cells by EPI or NE treatment (data not shown); however, a strong increase in ROS generation was detected using ROS-sensitive fluorescent dye DCFH in both cell types, which was blocked by the antioxidant *N*-acetyl cysteine (NAC) (Fig. 6*A*). EPI/NE-induced ROS generation was detected maximally between 0.5 and 1 h but reduced to basal level after 2 h of

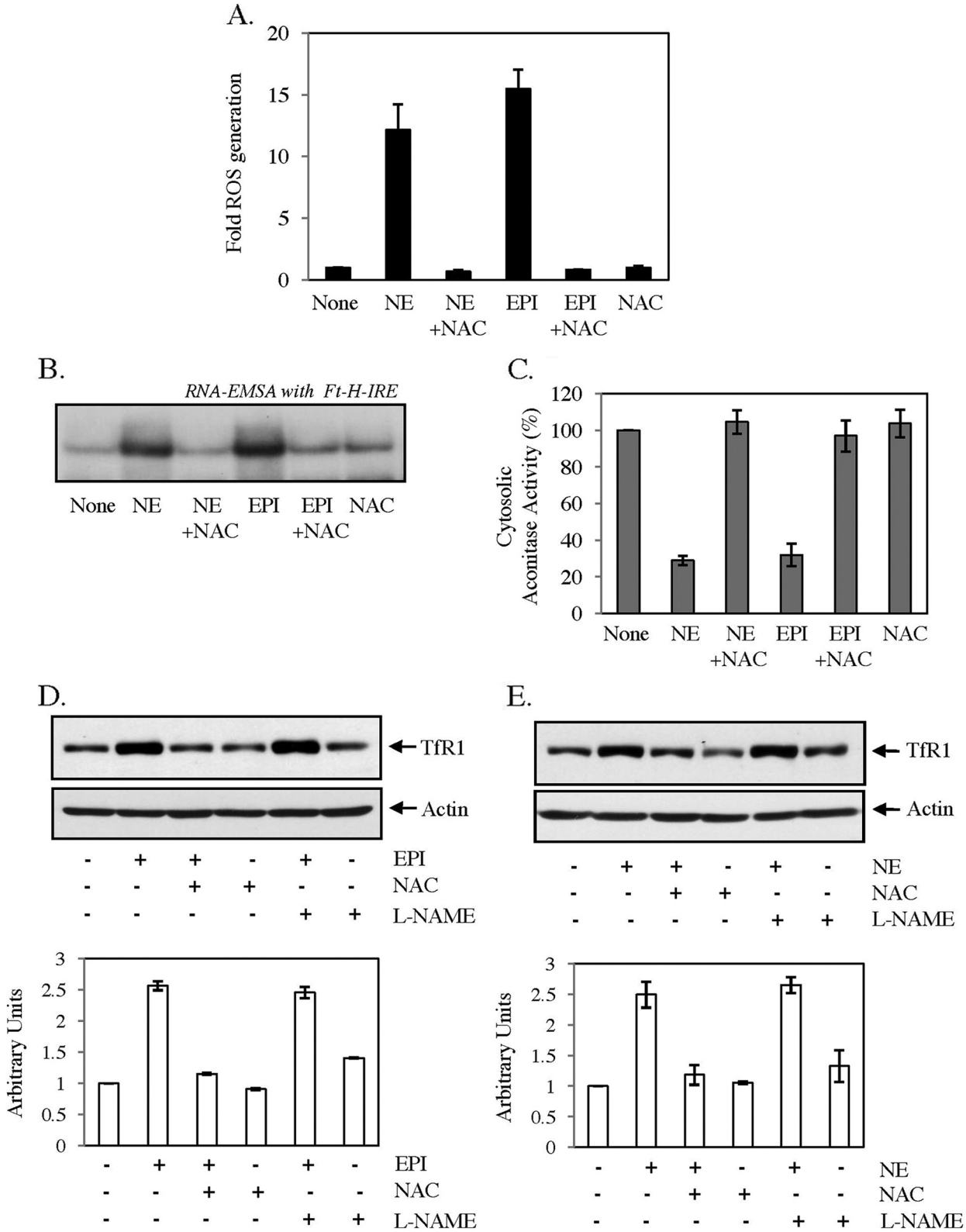

FIGURE 6. **Role of ROS in catecholamine-induced IRE-IRP interaction and TfR1 expression.** *A*, HepG2 cells were treated with medium alone (*None*), EPI (30 μM), or NE (30 μM) for 30 min, and intracellular ROS generation was detected by fluorescence microscopy using DCFH-DA as a substrate. NAC (7.5 mM) was added 30 min prior to the addition of EPI or NE. *B*, HepG2 cells were treated with 30 μM EPI or NE for 10 h or kept untreated (*None*). NAC (7.5 mM) was added 30 min prior to EPI/NE treatment. RNA gel-shift analysis was performed using cytosolic extracts and radiolabeled Ft-IRE probe. Data represent one of the three independent experiments. *C*, aconitase assay was performed in cytosolic extracts of medium alone (*None*) or EPI/NE (30 μM)-treated cells. NAC (7.5 mM) was added 30 min prior to catecholamine treatment. *D* and *E*, TfR1 (*upper panels*) and actin (*lower panels*) expressions in HepG2 cell lysates treated with either 30 μM EPI (*D*) or 30 μM NE (*E*) were analyzed by Western blot analysis. In both cases, cells were pretreated with NAC (7.5 mM) or L-N^G-nitroarginine methyl ester (*L-NAME*) (1 mM) for 30 min before the catecholamine treatment. TfR1 expression was quantified after normalization with actin (histograms below). *Error bars* indicate S.D. from three independent experiments.

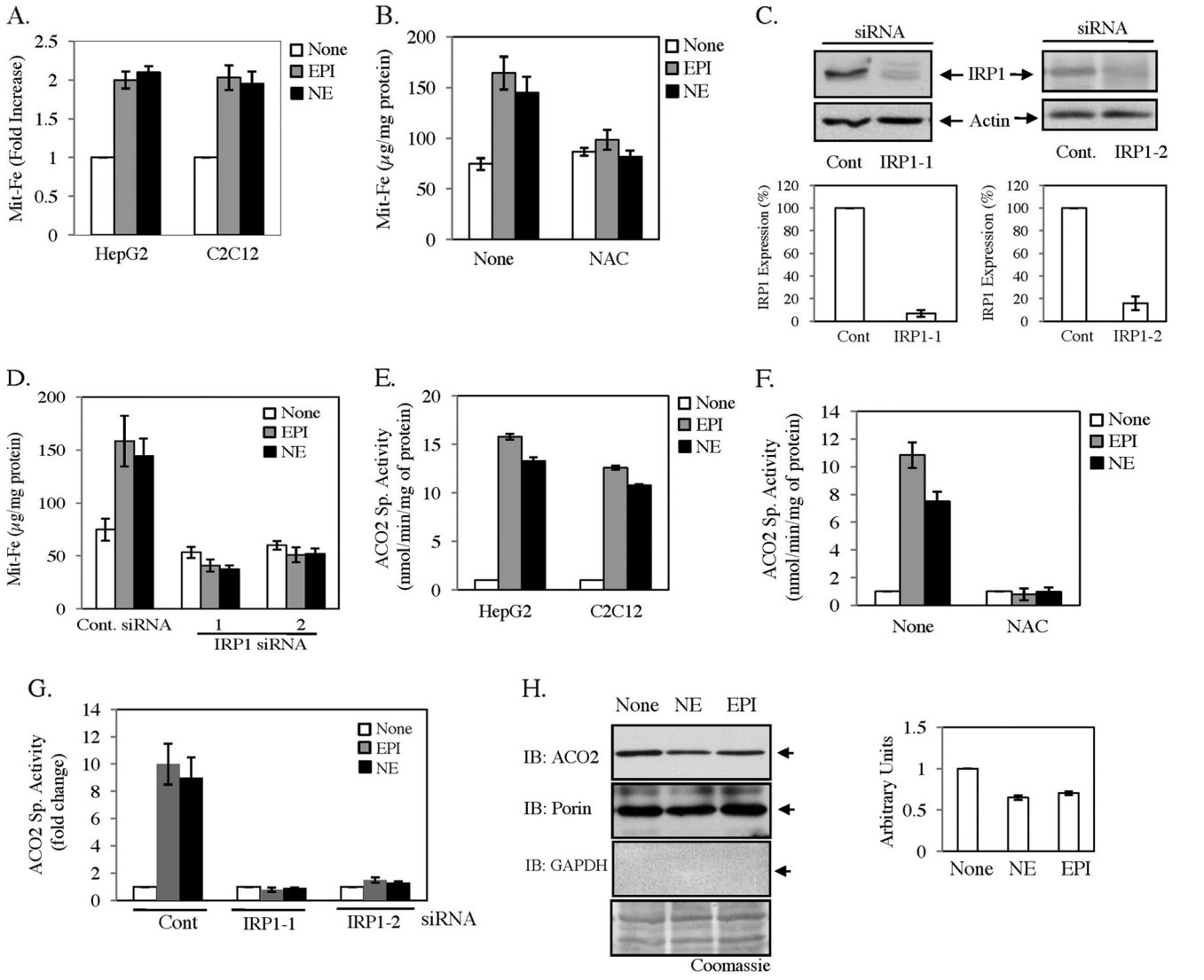

FIGURE 7. **Catecholamines increase mitochondrial iron content mediated by IRP.** *A*, HepG2 and C2C12 cells were treated with 30 μM EPI, NE, or medium alone (*None*). After 16 h, mitochondria were isolated ,and total iron was estimated using a standard. *B*, similarly, mitochondrial iron was estimated in HepG2 cells with prior treatment of 7.5 mM NAC for 30 min. *C*, HepG2 cells were transfected with control (*Cont*)- or IRP1-specific siRNAs (IRP1-1 and IRP1-2). After recovery, Western blot analysis was performed with either IRP1 or actin antibody. Densitometric analyses of these blots were shown in the *bottom panels*. *Error bars* indicate S.D. from three independent experiments. *D*, estimation of mitochondrial iron was performed in control- and IRP1 siRNA-transfected cells after treatment with 30 μM EPI/NE or medium alone (*None*) for 16 h. *E*, ACO2 specific activity (*ACO2 Sp. Activity*) was assayed in mitochondrial extracts isolated from HepG2 and C2C12 cells after treatment with 30 μM EPI/NE or medium alone (*None*) for 16 h. *F*, C2C12 cells were pretreated with 7.5 mM NAC for 30 min and then exposed to 30 μM EPI/NE or medium alone (*None*). After 16 h, an aconitase assay was performed on mitochondrial extracts. *G*, HepG2 cells were transfected with control- or IRP1-specific siRNAs, and an ACO2 activity assay was performed in mitochondrial extracts isolated from transfected cells after treatment with 30 μM EPI/NE or medium alone (*None*) for 16 h. *H*, Western blot analyses were performed in mitochondrial extracts with ACO2, porin, and GAPDH antibody after a 16-h treatment of medium alone (*None*) or EPI/NE (30 μM). The *bottom panel* shows the Coomassie Brilliant Blue-stained PVDF membrane after the blot (*IB*) was performed for GAPDH. The *side panel* represents densitometric analysis of ACO2 expression with porin as loading control from three independent experiments.

treatment (data not shown). NAC completely blocked EPI/NE-induced IRE-IRP binding (Fig. 6*B*) and altered cytosolic aconitase activity (Fig. 6*C*) in HepG2 cells. Moreover, EPI- (Fig. 6*D*) and NE (Fig. 6*E*)-induced TfR1 expression was completely blocked only by NAC but not by NO blocker L-N^G-nitroarginine methyl ester. All these results strongly suggest that EPI/NE-induced ROS generation is necessary for increased IRE-IRP interaction.

EPI and NE Promote Mitochondrial Iron Content and ACO2 Activity—A recent study suggests that the IRE-IRP system plays a crucial role in the mitochondrial iron management as IRP null mice suffer from mitochondrial iron deficiency in hepatocytes (9). Because we detected a strong activation of IRE-IRP system by EPI and NE, we estimated mitochondrial iron (Mit-Fe) content after EPI/NE treatment in both HepG2 and C2C12 cells. More than 2-fold increase in Mit-Fe content was detected in both cell types (Fig. 7*A*). The increase in Mit-Fe content was inhibited when HepG2 cells were pretreated with antioxidant NAC (Fig. 7*B*). Our earlier results (Fig. 5) suggest that IRP1 may play the predominant role in EPI/NE-induced IRE-IRP interaction. Thus, we blocked IRP1 expression in HepG2 cells by transfecting two different sets of IRP1-specific siRNA to determine its effect on EPI/NE-induced Mit-Fe content. We detected more than 90% decrease in IRP1 expression in IRP1-1 siRNA-transfected cells and an ~80% decrease in IRP1-2 siRNA-transfected cells than

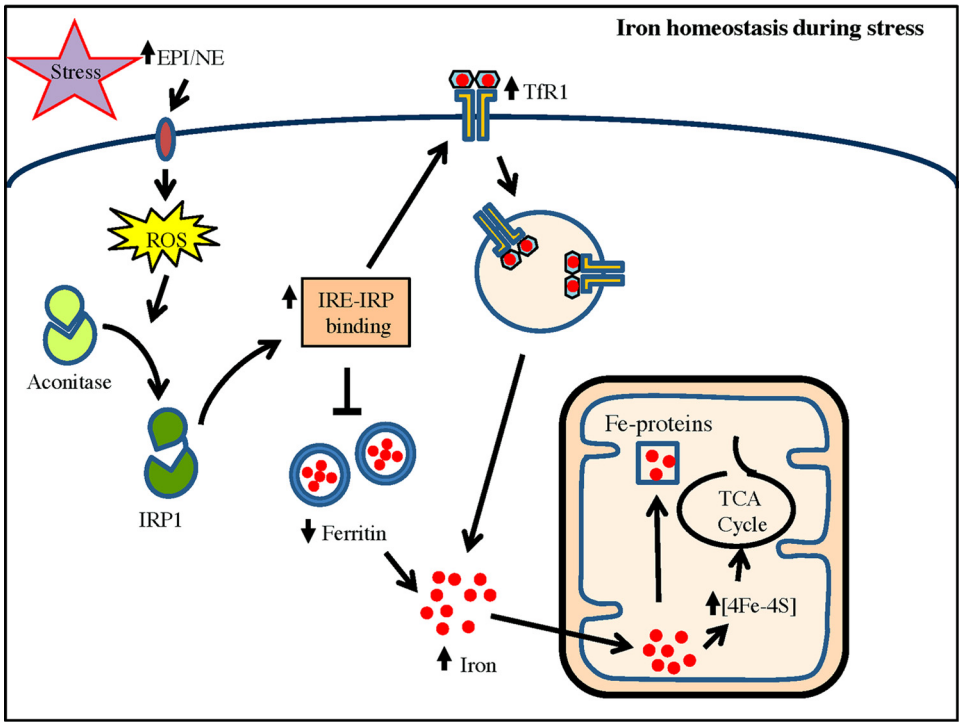

FIGURE 8. **A model suggesting the role of EPI/NE in iron homeostasis of hepatic/muscle cells.** Stress-induced release of EPI/NE binds to specific receptor to trigger intracellular ROS generation. ROS convert cytosolic aconitase to IRP1 that binds to IREs present in UTRs of TfR1 and ferritin to increase TfR1 mRNA stability and block ferritin translation, resulting in increase in the cellular iron pool. These events also promote mitochondrial iron content to increase the activity of iron-containing enzymes such as ACO2 of the TCA cycle, possibly to influence energy homeostasis in EPI/NE-exposed cells. Elevated mitochondrial iron may also be transported to other iron-containing mitochondrial proteins/enzymes (Fe-proteins) required for maintaining cellular homeostasis.

in control siRNA-transfected cells (Fig. 7*C*). The result showed that blocking of IRP1 expression inhibited EPI/NE-induced Mit-Fe content almost completely (Fig. 7*D*). Moreover, reduction of basal IRP1 expression also caused decreased Mit-Fe content even in untreated cells (Fig. 7*D*). It was earlier reported that cellular iron content regulates TCA cycle enzymes such as mitochondrial aconitase (ACO2) (1, 9); therefore, we determined ACO2 activity in mitochondrial extract isolated from EPI/NE-treated cells. ACO2 activity was increased up to 10–15-fold in both cell types (Fig. 7*E*), and this activity was blocked by NAC (Fig. 7*F*). Attenuation of IRP1 expression by siRNAs also blocked the increase in ACO2 activity (Fig. 7*G*). This result is in agreement with earlier findings that IRPs play the essential role for iron supplementation in mitochondria (9). Interestingly, increased IRE-IRP interaction should inhibit ACO2 expression due to the presence of an active IRE in its 5′-UTR (32). When we verified ACO2 expression by Western blot analysis, an ~35–40% decrease was detected by EPI/NE treatment (Fig. 7*H*), implying posttranslational iron incorporation for increased ACO2 activity due to EPI/NE exposure to cells. The purity of the mitochondrial fraction was determined by the presence of porin and absence of cytosolic protein GAPDH by Western blot analysis (Fig. 7*H*). All these results strongly suggest that EPI/NE regulate mitochondrial iron homeostasis by ROS-sensitive modification of IRE-IRP interaction.

DISCUSSION

Little is known regarding regulation of iron homeostasis in response to stress hormones such as EPI and NE. In this study, we found that EPI and NE both could increase IRE-IRP interaction to regulate iron homeostasis in hepatic and skeletal muscle cells. Increased IRE-IRP interaction, increased TfR1, and decreased Ft-H expressions were also detected in tissues of EPI- and NE-injected mice. This study also revealed that EPI/NE promotes mitochondrial iron supply through IRE-IRP interaction.

In mammals, EPI and NE regulate several enzymes of carbohydrate and lipid metabolism in various organs, including the liver and skeletal muscles, for energy generation (10, 11). They also increase activities of several enzymes participating in the TCA cycle and the electron transport chain (33, 34). For several of these enzymes, iron acts as cofactor. Thus, our finding of EPI and NE as direct regulators of iron homeostasis in liver and muscle cells is complementary with the physiological functions of these stress hormones. Our data may also explain iron overload detected in hepatic disorders, where the chronic release of catecholamines is part of the tissue repair response or defense against stress by the sympatho-adrenal medullary system (35, 36). Iron overload reported in liver diseases such as fibrosis and hepatocellular carcinoma (37, 38) may be caused by continuous exposure to elevated levels of catecholamines leading to gradual accumulation of iron.

IRPs are critical for maintaining cellular iron homeostasis by binding to IREs present in mRNAs of several iron homeostasis genes including TfR1, ferritin, and ferroportin. IRPs also regulate enzymes involved in cellular energy homeostasis such as ACO2 and succinate dehydrogenase (SDH) (32, 39, 40). We found that EPI or NE enhanced binding of IRP to the IREs present in the TfR1 3′-UTR to increase its transcript stability (Fig. 3*B*) and at 5′-UTR of Ft-H mRNA to block its translation (Fig. 3*C*). The coordinated regulation of TfR1 and ferritin

expressions in iron-depleted condition is well understood (41), but a similar regulation of TfR1 and ferritin due to increased IRE-IRP interaction by stress hormones has never been reported. The cellular iron exporter ferroportin also contains a single IRE in the 5′-UTR of its mRNA and is known to be regulated by cellular iron status (41, 42). Interestingly, we detected unaltered ferroportin expression by EPI (Fig. 1*E*) and ferroportin-IRE binding activity by catecholamines (Fig. 4*E*). No depletion in the cellular labile iron pool in EPI/NE-treated cells was detected by fluorescent dye calcein-AM (data not shown). This finding is consistent with earlier studies suggesting that ferroportin could be regulated only during iron deficiency-induced IRE-IRP interaction (43, 44). However, the reason for the failure of ferroportin-IRE-IRP interaction in response to EPI/NE is far from clear and needs future study. More importantly, unaltered ferroportin expression suggests the need for iron for intracellular metabolic activity in EPI/NE-treated cells. Our finding of increased mitochondrial iron content and ACO2 activity supports this view. Interestingly, ACO2 also contains a single IRE in its 5′-UTR (1, 32, 40). We detected decreased ACO2 protein levels in EPI/NE-treated cells (Fig. 7*H*), probably due to increased IRE-IRP interaction. However, ACO2 activity was increased more than 10 times in EPI/NE-treated cells (Fig. 7*E*), potentially due to its posttranslational modification from increased available iron to form [4Fe-4S] cluster (1, 9, 18). Blocking of increased ACO2 activity by antioxidant and IRP1 siRNA transfection (Fig. 7, *F–G*) further supports this view.

Among two cytosolic IRPs, the RNA binding activity of IRP1 is regulated by several factors, including cellular iron level, ROS (5, 30, 45), and nitric oxide (6, 7, 30), whereas IRP2 is regulated mostly by cellular iron level (8). We found that EPI- and NE-induced ROS generation decreased cytosolic aconitase activity and increased IRE-IRP interaction (Figs. 5 and 6), suggesting the predominant role of IRP1 in this mechanism. Unaltered IRP2 expression also supported this view (Fig. 5, *A*, *B*, *D*, and *E*). Blocking of EPI/NE-induced iron content of mitochondria and ACO2 activity by antioxidant NAC and IRP1 siRNA transfection (Fig. 7) also suggests that IRP1 alone may be sufficient in EPI/NE-mediated regulation of cellular iron homeostasis.

We detected a strong increase in fluorescence of the ROS-sensitive molecule DCF by EPI/NE, which was blocked by antioxidant NAC (Fig. 6*A*). Blocking of IRE-IRP interaction (Fig. 6*B*); decreased cytosolic aconitase activity (Fig. 6*C*); and increased TfR1 synthesis (Fig. 6, *D* and *E*) by NAC confirmed involvement of ROS. Moreover, NAC also completely blocked increased mitochondrial iron content and ACO2 activity (Fig. 7), suggesting that ROS generation is the key signal for EPI/NE-mediated regulation of cellular iron homeostasis. Catecholamines have been previously reported to generate ROS in different cell types (46, 47). Further study is needed to detect the cellular site of EPI/NE-mediated ROS generation or exact species involved in this mechanism.

In summary, our results show that stress hormones EPI and NE are potential regulators of cellular iron homeostasis. We reveal that EPI/NE promote mitochondrial iron content and ACO2 activity by ROS-mediated activation of IRP1 (Fig. 8). We speculate that this alteration of cellular iron homeostasis is necessary to adapt to changes associated with this catecholamine-induced metabolism and to restore energy balance.

REFERENCES

1. Oexle, H., Gnaiger, E., and Weiss, G. (1999) Iron-dependent changes in cellular energy metabolism: influence on citric acid cycle and oxidative phosphorylation. *Biochim. Biophys. Acta* **1413,** 99–107
2. Rouault, T. A., and Klausner, R. D. (1996) The impact of oxidative stress on eukaryotic iron metabolism. *EXS* **77,** 183–197
3. De Domenico, I., McVey Ward, D., and Kaplan, J. (2008) Regulation of iron acquisition and storage: consequences for iron-linked disorders. *Nat. Rev. Mol. Cell Biol.* **9,** 72–81
4. Ganz, T., and Nemeth, E. (2006) Regulation of iron acquisition and iron distribution in mammals. *Biochim. Biophys. Acta.* **1763,** 690–699
5. Hentze, M. W., and Kühn, L. C. (1996) Molecular control of vertebrate iron metabolism: mRNA-based regulatory circuits operated by iron, nitric oxide, and oxidative stress. *Proc. Natl. Acad. Sci. U.S.A.* **93,** 8175–8182
6. Kennedy, M. C., Antholine, W. E., and Beinert, H. (1997) An EPR investigation of the products of the reaction of cytosolic and mitochondrial aconitases with nitric oxide. *J. Biol. Chem.* **272,** 20340–20347
7. Soum, E., Brazzolotto, X., Goussias, C., Bouton, C., Moulis, J. M., Mattioli, T. A., and Drapier, J. C. (2003) Peroxynitrite and nitric oxide differently target the iron-sulfur cluster and amino acid residues of human iron regulatory protein 1. *Biochemistry* **42,** 7648–7654
8. Iwai, K., Klausner, R. D., and Rouault, T. A. (1995) Requirements for iron-regulated degradation of the RNA binding protein, iron regulatory protein 2. *EMBO J.* **14,** 5350–5357
9. Galy, B., Ferring-Appel, D., Sauer, S. W., Kaden, S., Lyoumi, S., Puy, H., Kölker, S., Gröne, H. J., and Hentze, M. W. (2010) Iron regulatory proteins secure mitochondrial iron sufficiency and function. *Cell Metab.* **12,** 194–201
10. Nonogaki, K. (2000) New insights into sympathetic regulation of glucose and fat metabolism. *Diabetologia.* **43,** 533–549
11. Viguerie, N., Clement, K., Barbe, P., Courtine, M., Benis, A., Larrouy, D., Hanczar, B., Pelloux, V., Poitou, C., Khalfallah, Y., Barsh, G. S., Thalamas, C., Zucker, J. D., and Langin, D. (2004) *In vivo* epinephrine-mediated regulation of gene expression in human skeletal muscle. *J. Clin. Endocrinol. Metab.* **89,** 2000–2014
12. De Boer, S. F., Koopmans, S. J., Slangen, J. L., and Van der Gugten, J. (1990) Plasma catecholamine, corticosterone and glucose responses to repeated stress in rats: effect of interstressor interval length. *Physiol. Behav.* **47,** 1117–1124
13. Kvetnansky, R., Sabban, E. L., and Palkovits, M. (2009) Catecholaminergic systems in stress: structural and molecular genetic approaches. *Physiol. Rev.* **89,** 535–606
14. Little, R. A., Frayn, K. N., Randall, P. E., Stoner, H. B., and Maycock, P. F. (1985) Plasma catecholamine concentrations in acute states of stress and trauma. *Arch. Emerg. Med.* **2,** 46–47
15. Esler, M., Jennings, G., Lambert, G., Meredith, I., Horne, M., and Eisenhofer G. (1990) Overflow of catecholamine neurotransmitters to the circulation: source, fate, and functions. *Physiol. Rev.* **70,** 963–985
16. Galli, A., Blakely, R. D., and DeFelice, L. J. (1998) Patch-clamp and amperometric recordings from norepinephrine transporters: channel activity and voltage-dependent uptake. *Proc. Natl. Acad. Sci. U.S.A.* **95,** 13260–13265
17. Blaak, E. E., Saris, W. H., and van Baak, M. A. (1993) Adrenoceptor subtypes mediating catecholamine-induced thermogenesis in man. *Int. J. Obes. Relat. Metab. Disord.* **17,** Suppl. 3, S78–S82
18. Richardson, D. R., Lane, D. J., Becker, E. M., Huang, M. L., Whitnall, M., Suryo Rahmanto, Y., Sheftel, A. D., and Ponka, P. (2010) Mitochondrial iron trafficking and the integration of iron metabolism between the mitochondrion and cytosol. *Proc. Natl. Acad. Sci. U.S.A.* **107,** 10775–10782
19. Das, N. K., Biswas, S., Solanki, S., and Mukhopadhyay, C. K. (2009) *Leishmania donovani* depletes labile iron pool to exploit iron uptake capacity of macrophage for its intracellular growth. *Cell. Microbiol.* **11,** 83–94
20. Drapier, J. C., and Hibbs, J. B. Jr. (1986) Murine cytotoxic activated macrophages inhibit aconitase in tumor cells: inhibition involves the iron-sulfur

prosthetic group and is reversible. *J. Clin. Invest.* **78,** 790–797
21. Tapryal, N., Mukhopadhyay, C., Das, D., Fox, P. L., and Mukhopadhyay, C. K. (2009) Reactive oxygen species regulate ceruloplasmin by a novel mRNA decay mechanism involving its 3′-untranslated region: implications in neurodegenerative diseases. *J. Biol. Chem.* **284,** 1873–1883
22. Biswas, S., Tapryal, N., Mukherjee, R., Kumar, R., and Mukhopadhyay, C. K. (2013) Insulin promotes iron uptake in human hepatic cell by regulating transferrin receptor-1 transcription mediated by hypoxia inducible factor-1. *Biochim. Biophys. Acta* **1832,** 293–301
23. Sierzputowska-Gracz, H., McKenzie, R. A., and Theil, E. C. (1995) The importance of a single G in the hairpin loop of the iron responsive element (IRE) in ferritin mRNA for structure: an NMR spectroscopy study. *Nucleic Acids Res.* **23,** 146–153
24. Dix, D. J., Lin, P. N., Kimata, Y., and Theil, E. C. (1992) The iron regulatory region of ferritin mRNA is also a positive control element for iron-independent translation. *Biochemistry* **31,** 2818–2822
25. Muralidharan, B., Bakthavachalu, B., Pathak, A., and Seshadri, V. (2007). A minimal element in 5′-UTR of insulin mRNA mediates its translational regulation by glucose. *FEBS Lett.* **581,** 4103–4108
26. Schwartz, J. W., Blakely, R. D., and DeFelice, L. J. (2003) Binding and transport in norepinephrine transporters: real-time, spatially resolved analysis in single cells using a fluorescent substrate. *J. Biol. Chem.* **278,** 9768–9777
27. Schwartz, J. W., Novarino, G., Piston, D. W., and DeFelice, L. J. (2005) Substrate binding stoichiometry and kinetics of the norepinephrine transporter. *J. Biol. Chem.* **280,** 19177–19184
28. Lok, C. N., and Ponka, P. (1999) Identification of a hypoxia response element in the transferrin receptor gene. *J. Biol. Chem.* **274,** 24147–24152
29. Taetle, R., Ralph, S., Smedsrud, S., and Trowbridge, I. (1987) Regulation of transferrin receptor expression in myeloid leukemia cells. *Blood* **70,** 852–859
30. Pantopoulos, K., Weiss, G., and Hentze, M. W. (1996) Nitric oxide and oxidative stress (H_2O_2) control mammalian iron metabolism by different pathways. *Mol. Cell. Biol.* **16,** 3781–3788
31. Rouault, T. A. (2006) The role of iron regulatory proteins in mammalian iron homeostasis and disease. *Nat. Chem. Biol.* **2,** 406–414
32. Kim, H. Y., LaVaute, T., Iwai, K., Klausner, R. D., and Rouault, T. A. (1996) Identification of a conserved and functional iron-responsive element in the 5′-untranslated region of mammalian mitochondrial aconitase. *J. Biol. Chem.* **271,** 24226–24230
33. Sylvia, A. L., and Piantadosi, C. A. (1985) *In vivo* modulation of norepinephrine-induced cerebral oxygenation states by hypoxia and hyperoxia. *Brain Res.* **338,** 281–288
34. Spencer, M. K., Katz, A., and Raz, I. (1991) Epinephrine increases tricarboxylic acid cycle intermediates in human skeletal muscle. *Am. J. Physiol.* **260,** E436–E439
35. Oben, J. A., and Diehl, A. M. (2004) Sympathetic nervous system regulation of liver repair. *Anat. Rec. A Discov. Mol. Cell Evol. Biol.* **280,** 874–883
36. Sancho-Bru, P., Bataller, R., Colmenero, J., Gasull, X., Moreno, M., Arroyo, V., Brenner, D. A., and Ginès, P. (2006) Norepinephrine induces calcium spikes and proinflammatory actions in human hepatic stellate cells. *Am. J. Physiol. Gastrointest. Liver Physiol.* **291,** G877–G884
37. Deugnier, Y., and Turlin, B. (2007) Pathology of hepatic iron overload. *World J. Gastroenterol.* **13,** 4755–4760
38. Philippe, M. A., Ruddell, R. G., and Ramm, G. A. (2007) Role of iron in hepatic fibrosis: one piece in the puzzle. *World J. Gastroenterol.* **13,** 4746–4754
39. Kohler, S. A., Henderson, B. R., and Kühn, L. C. (1995) Succinate dehydrogenase b mRNA of *Drosophila melanogaster* has a functional iron-responsive element in its 5′-untranslated region. *J. Biol. Chem.* **270,** 30781–30786
40. Gray, N. K., Pantopoulos, K., Dandekar, T., Ackrell, B. A., and Hentze, M. W. (1996) Translational regulation of mammalian and *Drosophila* citric acid cycle enzymes via iron-responsive elements. *Proc. Natl. Acad. Sci. U.S.A.* **93,** 4925–4930
41. Hentze, M. W., Muckenthaler, M. U., Galy, B., and Camaschella, C. (2010) Two to tango: regulation of mammalian iron metabolism. *Cell* **142,** 24–38
42. Abboud, S., and Haile, D. J. (2000) A novel mammalian iron-regulated protein involved in intracellular iron metabolism. *J. Biol. Chem.* **275,** 19906–19912
43. Lymboussaki, A., Pignatti, E., Montosi, G., Garuti, C., Haile, D. J., and Pietrangelo, A. (2003) The role of the iron responsive element in the control of ferroportin1/IREG1/MTP1 gene expression. *J. Hepatol.* **39,** 710–715
44. Eisenstein, R. S., and Ross, K. L. (2003) Novel roles for iron regulatory proteins in the adaptive response to iron deficiency. *J. Nutr.* **133,** 1510S–1516S
45. Caltagirone, A., Weiss, G., and Pantopoulos, K. (2001) Modulation of cellular iron metabolism by hydrogen peroxide. Effects of H_2O_2 on the expression and function of iron-responsive element-containing mRNAs in B6 fibroblasts. *J. Biol. Chem.* **276,** 19738–19745
46. Remondino, A., Kwon, S. H., Communal, C., Pimentel, D. R., Sawyer, D. B., Singh, K., and Colucci, W. S. (2003) β-adrenergic receptor-stimulated apoptosis in cardiac myocytes is mediated by reactive oxygen species/c-Jun NH_2-terminal kinase-dependent activation of the mitochondrial pathway. *Circ. Res.* **92,** 136–148
47. Gupta, M. K., Neelakantan, T. V., Sanghamitra, M., Tyagi, R. K., Dinda, A., Maulik, S., Mukhopadhyay, C. K., and Goswami, S. K. (2006) An assessment of the role of reactive oxygen species and redox signaling in norepinephrine-induced apoptosis and hypertrophy of H9c2 cardiac myoblasts. *Antioxid. Redox. Signal.* **8,** 1081–1093